Toward New Low-Temperature Thermochemical Heat Storage Materials: Investigation of Hydration/Dehydration Behaviors of $MgSO_4$/Hydroxyapatite Composite

Minh Hoang Nguyen [1,2], Mohamed Zbair [1,2], Patrick Dutournié [1,2], Antonella Gervasini [3], Cyril Vaulot [1,2], and Simona Bennici [1,2,*]

[1] Université de Haute-alsace, CNRS, IS2M UMR 7361, F-68100 Mulhouse, France; minh-hoang.nguyen@uha.fr; mohamed.zbair@uha.fr; patrick.dutournié@uha.fr; cyril.vaulot@uha.fr; simona.bennici@uha.fr

[2] Université de Strasbourg, France

[3] Dipartimento di Chimica, Università degli Studi di Milano, via Camillo Golgi, 19, 20133 Milano, Italy, antonella.gervasini@unimi.it

*Corresponding author: simona.bennici@uha.fr; Tel.: +33 (0)3 89336729

Highlights

- $MgSO_4$-hydroxiapatite composite materials were synthesised using impregnation method.
- Physical characteristics of different composite materials were characterized.
- Hydration kinetic and water uptake of different samples were investigated.
- Composite salt of 20 wt% has a good stability over 20 hydration/dehydration cycles.

Abstract:

A new two-component (composite) water sorbent $MgSO_4$/Hydroxyapatite has been developed for sorption-based solar heat storage. The matrix of the composite is a hydroxyapatite (HAP) material with ordered structure, high surface area of 111.3 m^2/g and mesopore dimensions centered at 45 nm. The composites, prepared by wet-impregnation of HAP with $MgSO_4$, have lower specific surface area and similar mesopore dimensions as the matrix. The maximum water sorption capacity of HAP is 0.039 g/g, while the composite (20-$MgSO_4$/HAP) possesses 3.7 times higher maximum

water sorption capacity due to the presence of the salt in the matrix. The HAP composite containing 20% $MgSO_4$ achieved the highest heat of hydration 464 J/g. A long-term cycling (dehydration at 150 and hydration at 30 °C at a relative humidity of 60%) confirms a comparatively good stability of the composite.

Keywords: Thermochemical storage of solar heat; magnesium sulfate; hydroxyapatite; water sorption; adsorption kinetics.

1. Introduction

Solar energy is considered a viable alternative to conventional energy sources, and its potential applications in residential and industrial surroundings have been extensively studied [1,2]. Though, the imbalance between energy supply and demand makes it difficult to put into practice. Thermal energy storage (TES) is an evolving technology and an effective way to achieve long-term solar energy use [3,4]. Latent heat storage, sensible heat storage, and thermochemical heat storage (TCHS) are three types of system using TES technologies. While latent and sensible heat storage have been extensively studied in recent decades [5,6], there have been few studies on TCHS, which is highly competitive and have been attracting growing interests due to higher energy storage density and negligible heat loss over long storage periods [7,8]. Based on the reversible sorption reaction, heat is stored following the endothermic reaction (charging) and this energy can be retrieved later on from the exothermic reaction (discharging) for many practical applications in particular in the building sector. In these application the most common configuration is based on the sorption phenomena of a sorbate (often water) on a sorbent (generally a solid material).

The solid thermochemical storage material has to be chosen carefully to ensure a good working system. Basically, it must possess certain properties such as high energy density, high affinity for the sorbate (water in most cases), a high mass and heat transfer with a charging temperature as low as possible to fit in residential applications

[9,10]. In addition, the material needs to be eco-friendly, non-toxic and inexpensive. With these criteria, salt hydrates appear to be a promising storage materials [11]. $SrBr_2$, $MgCl_2$, and $MgSO_4$ hydrates are among the best potential salt hydrates, with $MgSO_4$ hydrate having the highest theoretical heat storage density of 2.8 GJ/m^3 and a low charging temperature (<150 °C), which is suitable for building applications with solar collectors, being the most cost-effective [12,13], and, most importantly, having a dehydration temperature that matches well with the thermal solar collectors. Furthermore, to broaden the applications panel, the salt's relative humidity of deliquescence (RHD) is a crucial metric to consider. The RHD is the relative humidity limit at which the salt will dissolve in the adsorbed water in proportion to temperature, resulting in absorption into the material. Excessive water absorption permits more water to be absorbed, increasing the amount of heat generated by the process. The production of saline solution, on the other hand, might produce corrosion issues [14]. The deliquescence process of $MgSO_4$, nH_2O, for example, will not occur below 80% relative humidity (RH) at temperatures ranging from 10 to 80 °C since it is thermodynamically stable at this temperature and humidity range [15,16]. The major drawbacks of this system are the overhydration, the formation of aggregates occurring during rehydration, the kinetic hindrance limiting the mass and heat transfer, and the poor cyclability [15]. Consequently, the system's full potential could not be reached and, as a result of these constraints, the energy storage capacity was low. One way to take advantage of the $MgSO_4$'s great potential is to make composites by dispersing the salt in a porous matrix to avoid swelling and aggregates formation, which represent one of the main materials' drawbacks. To overcome these issues, efforts have been focused on the development of high-performance composite materials using porous matrix and salt hydrates [11,17].

The composite sorbents are also known as "composite salt in porous matrix" (CSPM), a term used by Yuri Aristov et al. [18]. However, if composite sorbents are subjected to a wet environment for an extended period of time and the collected water is

insufficient to be held inside the pores, they are at risk of solution leakage. As a result, developing a porous matrix with an ultrahigh pore volume to load a high content of salts and store a big amount of collected water is extremely important in order to avoid the risk of liquid leakage.

For that reason, several sorbent materials as a matrix for hydrated salts, such as silica gel [19,20], activated alumina [21], zeolite [22,23], MOFs [24], vermiculite [25], and expanded graphite [26,27], has received considerable attention. However, in order to be an appropriate material for TES applications, the matrix must fulfill a number of criteria, including cheap cost, a low regeneration temperature, a high storage density, and good mass and heat transfers that enable long-term storage with high efficiency and an easier recovery of the heat by different means (air vector, solid/liquid, solid/air heat exchangers).

Despite the fact that a variety of innovative composite sorbents for heat storage have been developed [24,28–32], there is still a significant gap between the materials and their practical applications. As supporting matrices, for example, different zeolites, which are aluminosilicate minerals having microporous structures for moisture adsorption, are commonly used. Wang et al. [22] performed the solution impregnation approach to create the $MgSO_4$@zeolite-13x composite thermochemical sorbent. They indicated that the sorbent contained 8% by weight $MgSO_4$ performed better at a high RH of 80%, with no salt crystals visible on the surface. However, the low ESD of about 600 J/g and cyclability need to be further improved. $MgSO_4$@zeolite has been proven to be financially viable for home interseasonal energy storage, however it may not entirely fulfill a household's heating requirement [30]. The adsorption capacity of $MgSO_4$@zeolite sorbent, on the other hand, would considerably decrease if the hydration temperature is above 50 °C [4], implying that the maximum discharge temperature in the application would not exceed 50 °C. Zhang et al. [33] produced a range of form-stable cylindrical structures using zeolite-13X as a matrix. The sample with the optimal mass ratio (zeolite-13X: $CaCl_2$: $MgSO_4$ = 10: 54: 36) exhibited a

gravimetric-ESD of 1410 J/g at a dehydration temperature of 250 °C, and the value reduced by 20% after 20 dehydration-hydration cycles. Although zeolites are common and inexpensive matrices, inherent defects such as a high charging temperature (>200 °C) and a low thermal conductivity.

Aristov et al. [18] studied different composites by embedding hygroscopic salts (e.g., $CaCl_2$ and LiBr) in mesoporous and microporous silica gels. The salts were distributed rather than bulk, which helps to reduce swelling and agglomeration and to speed up mass and heat transmission. The pore structure and chemical content of the host matrix materials have a significant impact on the heat storage capacity of salt/porous matrix composites [34], therefore choosing the right host porous material is crucial. By impregnating $CaCl_2$ into SBA-15 pores, Ponomarenko et al. [35] produced a composite material that could adsorb 0.47 g/g. Courbon et al. [36] presented an improved synthesis process for silica gel and $CaCl_2$ composites. The energy storage density was 300 Wh/kg, and the cycle loading uptake was 0.4 g/g. Whiting et al. [37] investigated the use of zeolite as a porous matrix to increase $MgSO_4$ heat storage. When impregnated with $MgSO_4$, the zeolite Na–Y with the largest surface area (780 m^2g^{-1}) and total pore volume (0.32 cm^3g^{-1}) produced the highest heat of hydration (1090 J/g). The water sorption process on expanded vermiculite/$CaCl_2$ composites was researched by Aristov and coworkers [38], who claimed that impregnation of $CaCl_2$ into expanded vermiculite can increase the water sorption capacity even at low water vapor pressure. However, expanded vermiculite's surface area is low (9 m^2g^{-1}), making it unsuitable for salt loading and mass transfer. Although these porous materials can increase the heat storage capacity of organic salts, they have low pore size and it is hard to modulate their structures and properties.

Shi et al. [24] made-up $CaCl_2$-based metal-organic frameworks (MOFs) composites with a high storage energy of 1274 J/g with moderate stability via 17 continuous adsorption/desorption cycles. Palomba and coworkers encapsulate LiCl into silica gel to improve the dynamic behavior of a long-term adsorption heat storage with a maximum useful heat of 450 J/g [39]. Calabrese [40] designed a silicone foam/$MgSO_4$

141 composite and shown that this material improved mechanical stability and cycle
142 performance considerably.

143 It is obvious from the above literature study that there are still improvements to be
144 made in TES materials for heat storage. Certainly, the studies on composites appear to
145 be too diverse. However, various flaws, such as vermiculite's low heat conductivity,
146 zeolite's high desorption temperature, and MOFs' poorer thermo-mechanical
147 characteristics, must be addressed.

148 The type of porosity (micro/meso) is a significant element in composite design,
149 according to these studies. The salt may plug the pores if they are too tiny, preventing
150 water molecules from diffusing and lowering energy storage capacity. Other materials,
151 such as mesoporous activated carbon or silica-gels, have also been shown to be
152 excellent supports. Salt may be incorporated through their large pores, increasing their
153 energy storage capacity while preventing pore obstruction [41,42]. Aside from the high
154 surface area and the existence of mesoporosity, strong thermal conductivity is a
155 significant consideration in selecting the best support. This parameter is critical for the
156 heat transport phenomena to be optimized.

157 A porous host matrix with a large pore size structure (mesoporous) is needed to
158 improve the composite material's water uptake. In this study, in addition to the
159 commonly used porous materials (zeolites, silica gel, and so on), a new host matrix is
160 used: hydroxyapatite (HAP), a calcium phosphate apatite with a developed
161 mesoporous structure [43].

162 HAP - $Ca_{10}(PO_4)_6(OH)_2$, is a well-known biomaterial of the calcium phosphate family
163 with high biocompatibility. Recently, Hu et al. [44] discovered that a HAP nanowire
164 membrane could be used as a separator, especially for high-temperature Li-ion battery
165 applications. Because of its low cost, superior compatibility with surrounding
166 materials, and higher adsorption ability, nanoscale HAP is regarded as one of the most
167 significant biomaterial adsorbents. HAP can be used also as an adsorbent to absorb
168 heavy metal ions like Pb^{2+}, Cu^{2+}, and Cd^{2+}, which are attributed to the ion Ca^{2+} in

solution through metal cations [45]. HAP is also regarded as one of the most promising adsorption materials for absorbing different organic and inorganic pollutants [46]. Amedlous et al. [47] have been used natural mesoporous hydroxyapatite as support for copper loading as eco-friendly Fenton-like catalyst to effectively remove organic dyes. Furthermore, Wang et al. [48] determined that HAP has a thermal conductivity of 0.15 to 0.20 W/m K, indicating that it has a high heat transfer capacity. As a consequence, employing HAP as a porous matrix for hygroscopic salts is valuable, as it will allow to better understand water sorption and heat transport in composite materials.

For all the above-mentioned reasons and to the best of our knowledge, this is the first work which reports the use of HAP as adsorbent in TCHS application. Incorporation of $MgSO_4$ in HAP matrix may increase the total charge storage capacity and potentially overcome its limitations. In addition, the HAP shows a low density and mesoporous structure, which is very conducive to its application in TCHS system [49]. The OH- group in HAP can form hydrogen bonds with water which inhibits the leakage of the salt [48]. In this study, composites designed by impregnation of $MgSO_4$ on a HAP support were prepared, characterized, and their performance assessed. In addition to the heat of hydration released, the experimental kinetic data were examined. The goal was to produce composite materials with high energy density storage with a fast reaction kinetics.

2. Materials and Methods

2.1. Composite materials preparation

2.1.1 Hydroxyapatite (HAP) preparation

Hydroxyapatite synthesis was carried by using pure reagent-grade salt precursors, namely, calcium nitrate tetra hydrate, $Ca(NO_3)_2{\cdot}4H_2O$ (>99.0% from Merck ACS); and ammonium dihydrogen phosphate, $(NH_4)H_2PO_4$ (>98.0% from Sigma-Aldrich).

Stoichiometric hydroxyapatite was synthesized by the conventional co-precipitation method by fixing the Ca/P molar ratio of the reagents in solution at 1.67, operating by the procedure reported in Campisi work [50]. For the preparation of ca. 4 g of stoichiometric hydroxyapatite, 250 mL of an aqueous solution containing 0.167 mol of $Ca(NO_3)_2 \cdot 4H_2O$ was added to 250 mL of a 0.1 mol of $(NH_4)H_2PO_4$ solution placed in a 4-neck round flask and maintained under stirring at 80°C. During the synthesis, the pH value was maintained at value of 10 by an appropriate addition of a 28-30% NH_4OH solution (from Sigma-Aldrich). The formed precipitate was slowly filtered, washed with hot water, and dried first at 50 °C under vacuum and then at 120 °C for 8 h. The grain size of HAP obtained is in the range of 0.5-1 mm with a density of 3.16 g/cm^3.

2.1.2 Composite materials ($MgSO_4$/HAP) preparation

Incipient Wetness Impregnation (IWI) method [51] was used for embedding $MgSO_4$ ($MgSO_4 \cdot 7H_2O$ 99.9 % from Sigma-Aldrich) inside HAP adsorbent. This traditional method consists of only filling the pores of the HAP with an aqueous solution of $MgSO_4$. To do this, the HAP support was firstly oven-dried at 150 °C to remove any trace of water from the pores. An aqueous solution of $MgSO_4$ was then applied on the dried support (room temperature and pressure) until it starts to get wet. The impregnated materials were then dried at 150 °C for 12 h. Accordingly, two composites were prepared by IWI and then labelled as x-$MgSO_4$/HAP (1st column in **Table 1**) with x is the theoretical content of $MgSO_4$ in the composites. The first composite contains 5 wt% of $MgSO_4$ and the second one contain 20 wt% of $MgSO_4$ which is the maximum amount that can be integrated inside HAP. The experimental salt content was determined by means of X-Ray Fluorescence. The density of HAP is 3.16 g/cm^3 and the density of anhydrous $MgSO_4$ is 2.66 g/cm^3. With the law of mixture, the density of the composites would be 3.07 g/cm^3 for the 20-$MgSO_4$/HAP and 3.14 g/cm^3 for the 5-$MgSO_4$/HAP.

2.2. Physicochemical characterizations methods

X-Ray Diffraction (XRD) analyses were performed on the compacted powder of the samples on a diffractometer PANalytical MPD X'Pert Pro, equipped with a Pixcel real-time multiple strip detector, operating with an angular aperture of 3.347° 2θ in 3° to 80° 2θ range, and using CuKα radiation with 0.15418 nm wavelength. Diffractograms were recorded at 22 °C with a step size of 0.013° 2θ and a scan time of 220 s per step.

A wavelength dispersion X-Ray Fluorescence (WDXRF) spectrometer (from PANalytical, Zetium) was used to perform the XRF measurements on pellets made of 0.2 g of the sample.

High-resolution micrographics were acquired by a Scanning Electron Microscope (SEM) from JEOL, JSM-7900F model. The semi-quantitative chemical analysis and atomic composition mapping of the sample was performed by means of Energy Dispersive X-ray (EDX).

N_2 adsorption/desorption isotherms of support and composites at -196 °C were acquired in a ASAP 2420 device from Micrometrics (Micromeritics, Norcross, GA, USA). The samples were previously degassed at 150 °C for 12 h and then, again at 150 °C for 2 h directly in the calorimetric cell before analysis. The specific surface area was calculated applying the Brunauer, Emmett and Teller (BET) equation (S_{BET}) ($0.01<p/p°<0.40$). The mesoporous volumes (V_m), external surface (ext) and microporous surface (S_m) were determined by applying the t-plot method (thickness range: 0.35-0.50). Finally, the pore size distribution (PSD) was determined using Barrett, Joyner and Halenda (BJH) method applied on the desorption branch of the isotherms.

2.3. Hydration/dehydration experiments

A Sensys TG-DSC (Thermogravimetry coupled to differential scanning calorimetry) apparatus, equipped with a Wetsys flow humidity generator both from Setaram (**Figure 1**) were used to measure the heat released and the water adsorption amounts (measured by the microbalance) of the HAP and its composites. Prior to the hydration process, the samples (~10 mg) were dehydrated at 150 °C by increasing the temperature from 30 to 150 °C at 5 °C/min under a flow of dry air (30 mL/min) with a subsequent isotherm of 3 h at 150 °C to ensure a complete dehydration. Then, each sample was cooled down to 30 °C and, once having attained a stable thermal (DSC signal) baseline, the relative humidity (RH) of the air flow was increased to 60 % (equivalent to a water vapor partial pressure of 2.55 kPa). The hydration process was set for 8 hours in order to completely rehydrate the material – the complete rehydration was reached when the DSC signal returned to the baseline. **Figure 2a** depicts the temperature profile used for all the calorimetric experiments. These conditions were selected to be as close to a real-life residential application as possible: 150 °C is the average working temperature that can be reached using a flat-plate solar heat collectors [37,52] and 30 °C is close to the indoor air temperature during the discharging phase [53]. To accurately calculate the dehydration/hydration heat, the dehydration/hydration process for each sample was performed after stabilizing the DSC and TGA signals. Blank experiments with empty crucibles in the same conditions were also performed. The signals (DSC and TGA) of the blank experiment were then subtracted from the sample experiment. The dehydration/hydration heat (J/g_{sample}) were finally obtained by integrating the surface of the subtracted curves (see **Figure 2b** as an example).

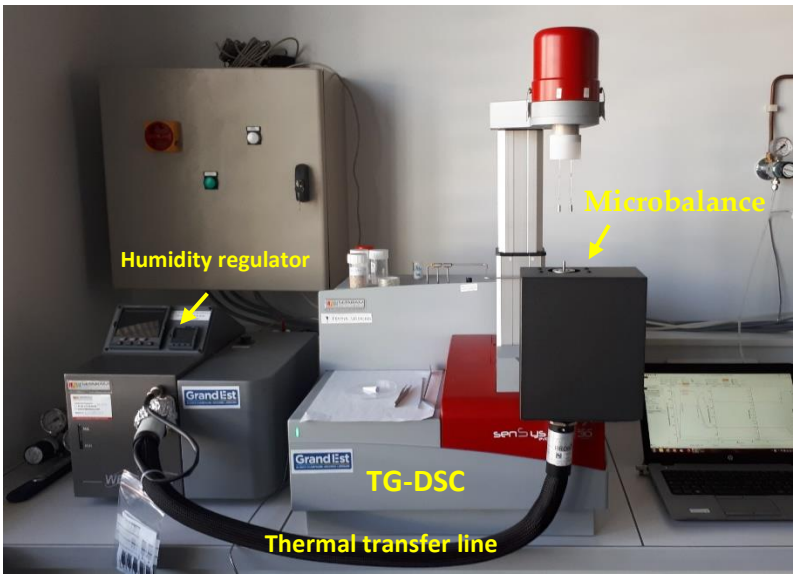

272

273 **Figure 1.** A Sensys TG-DSC apparatus equipped with a microbalance and connected to a
274 humidity regulator Wetsys by a thermal transfer line (from Setaram).

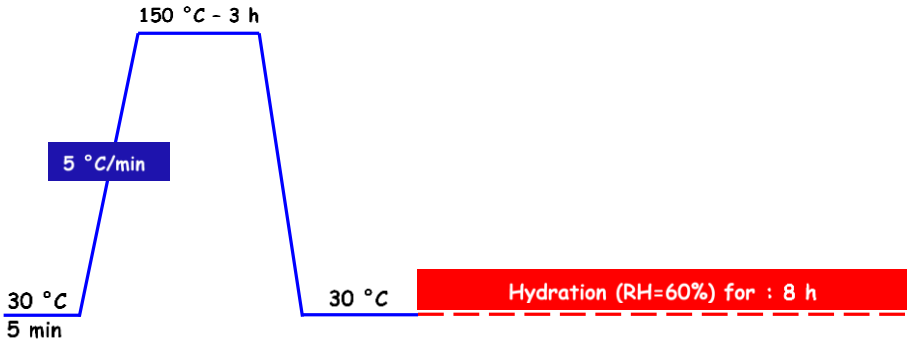

275

276 **Figure 2a.** Thermal cycle used for the TG-DSC/WETSYS analyses.

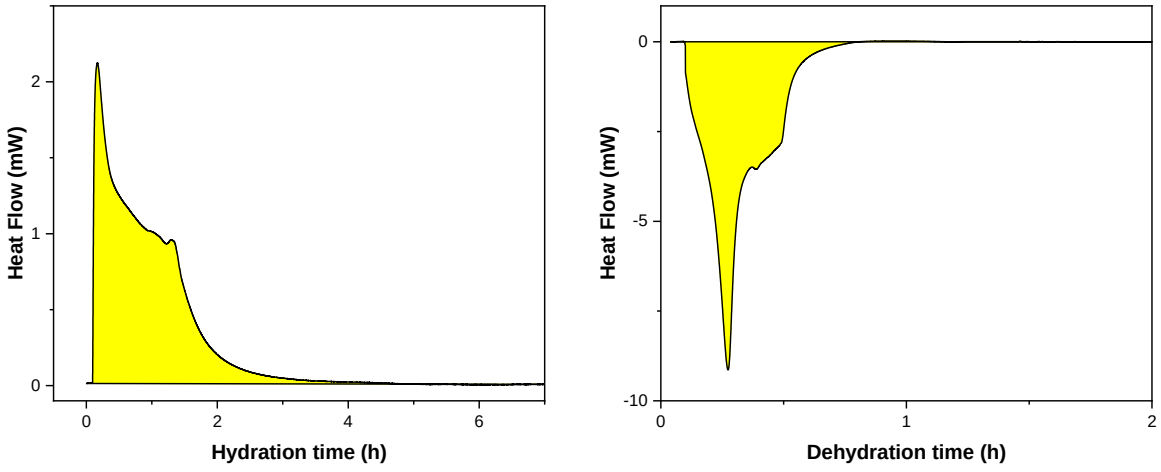

277

Figure 2b. Example of DSC peaks for hydration and dehydration (after subtraction of the blanck analysis performed in the same conditions) for the 20-$MgSO_4$/HAP sample. The (yellow area) represents the heat.

3. Results and discussion

3.1. Structural properties of the composite materials

Table 1 summarizes the chemical composition obtained using the WDXRF method as well as the textural parameters (S_{BET}, S_{ext}, S_m, V_p, and V_{meso}, where S_{ext} is the external surface and V_{meso} is the mesoporous volume). With increasing $MgSO_4$ loading, the S_{BET} and V_p (total pore volume) values of the HAP and related composites show a significant decrease. This might be explained by the pore blocking by $MgSO_4$ and then a decrease in the pore accessibility by the N_2 molecules. Actually, the initial Vp (0.664 cm^3/g) diminished by 25% (0.499 cm^3/g) after the impregnation of 4.11% $MgSO_4$, and it shrank to only 0.358 cm^3/g after HAP was incorporated by 17.27% $MgSO_4$. HAP support and prepared composites display type IV isotherm according to Ref. [54]. We can observe that the deposition of $MgSO_4$ do not impact the isotherm shape even if by increasing the quantity of impregnated salt, the adsorbed volumes decrease. (**Figure 3a**). The adsorption curves appear slightly convex at a very low p/p° (insert in **Figure 3a**), representing a minor part of microporosity in the different materials (Type I isotherm). A type IV isotherm is particularly identified by capillary condensation/evaporation at high relative pressures (from 0.8 – 1.0 p/p°) interpreted by a hysteresis loop. In the present cases, the adsorption and desorption branches appear relatively parallel, and the phenomena seems to finish at about p/p° = 0.8. This behavior is relatively typical of type H1 hysteresis [55]. The type IV isotherm with a type H1 hysteresis and the p/p° range of the hysteresis highlight the presence of mesopores (eventually macropores) with a large distribution in the porous structure of the composite. The pore size distribution (PSD) of the composites and pure HAP shown in **Figure 3b** has been obtained by applying the BJH method to the desorption branches of N_2 adsorption/desorption isotherms [56]. The composites maintain the

same unimodal, but large (between 10 and 200 nm), distribution as the HAP (only the pore volume is diminished) with peaks centered at around 45 nm. This distribution confirms the predominance of the large mesopores and macropores in the composites porous structures. Since the PSD of the composites is maintained, the size of the pore entrance is not affected. This result suggests the filling and complete blocking of several pores by aggregates of salt particles; no narrowing of the pores due to the deposition of salt can be deduced.

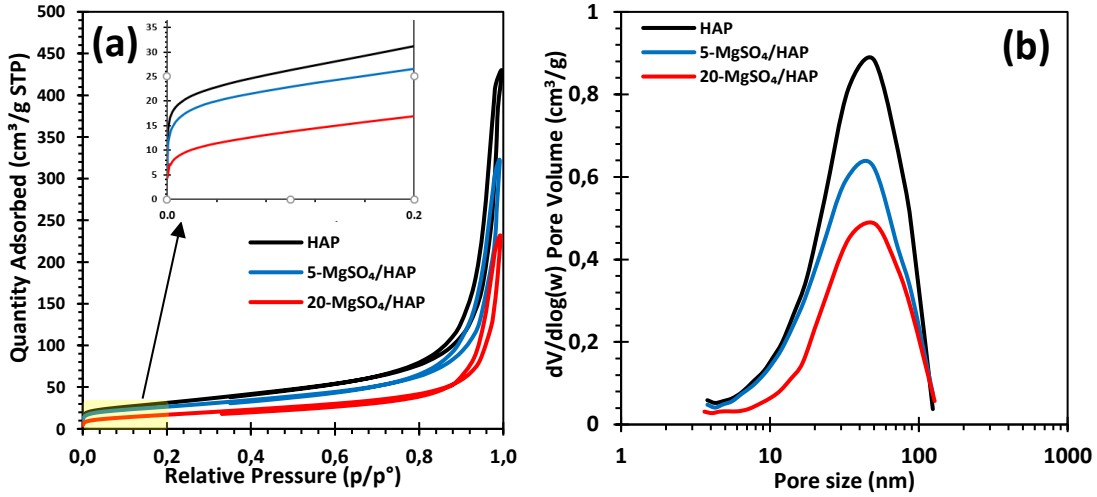

Figure 3. (a) N_2 adsorption-desorption isotherms and **(b)** pore size distribution of HAP and its composites with $MgSO_4$.

Table 1. Physicochemical characteristics of HAP support and $MgSO_4$/HAP composites.

Sample	$MgSO_4$ content (wt%)	S_{BET} ($m^2.g^{-1}$) [a]	S_{ext} ($m^2.g^{-1}$) [b]	S_m ($m^2.g^{-1}$) [b]	V_p ($cm^3.g^{-1}$) [c]	V_{meso} ($cm^3.g^{-1}$) [b]
HAP	-	111.3	99.6	11.7	0.664	0.659
5-$MgSO_4$/HAP	4.11	93.9	83.3	10.6	0.499	0.494
20-$MgSO_4$/HAP	17.27	63.1	63.1	0	0.358	0.358

[a] Calculated using the BET equation at p/p° between 0.01 and 0.40.

[b] Determined using the *t*-plot method with thickness range 3.5-5 Å.

[c] Determined from the amount of N_2 adsorbed at p/p°=0.99.

The crystallinity and phase identification of the prepared samples were determined using XRD. The XRD patterns of all samples (**Figure 4a**) revealed a pure HAP phase ($Ca_{10}(PO_4)_6(OH)_2$), with all reflections identical to the reference database (ICDD 00-064-0738). Nonetheless, an unidentified peak at around 20° 2θ was observed on the XRD pattern of 20-$MgSO_4$/HAP (**Figure 4a**). To verify the source of such peak, the sample was exposed to ambient air for 30 hours. Further hydration occurred, and then the intensity of this peak increased alongside the appearance of additional peaks between 17-20° 2θ (**Figure 4b**). These peaks have been identified using database of X'Pert HighScore Plus software and they were assigned to $MgSO_4.6H_2O$ (ICDD 00-024-0719) (**Figure 4b**). On the other hand, no additional $MgSO_4$ reflections were observed in the XRD patterns, suggesting that an amorphous $MgSO_4.yH_2O$ phase ($y < 6$) could be present in the sample [57]. In fact, the amorphicity of the $MgSO_4.yH_2O$ phase was confirmed after analyzing the diffractograms of $MgSO_4$ during the dehydration process up to 150 °C (**Figure 4c)**. At first, at 25 °C the sample showed high crystallinity. Then the degree of crystallinity gradually decreased increasing the temperature at 44 °C and 55 °C. Finally, the diffractogram shows no crystallinity between 80 and 150 °C. Furthermore, the dehydration was incomplete at this point, leading to the fact that there are amorphous hydrated phases present. This could be related to the blocking of the pores which hinders the initial dehydration (after impregnation) of the hydrated salt confined in the porous structure [37]. Another suggestion is that the $MgSO_4$ crystallites could be smaller than the detection limit of the XRD spectrometer and so, no well-defined peaks are observed on the XRD patterns.

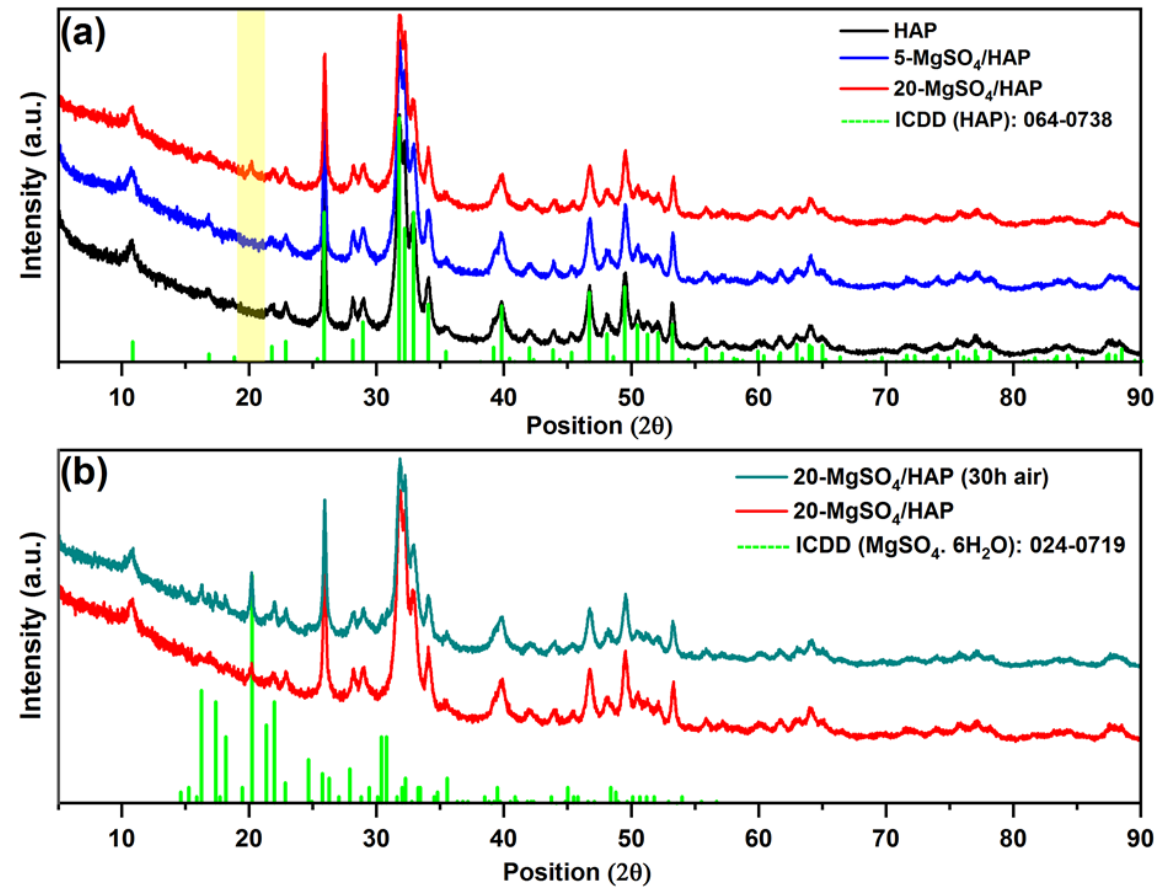

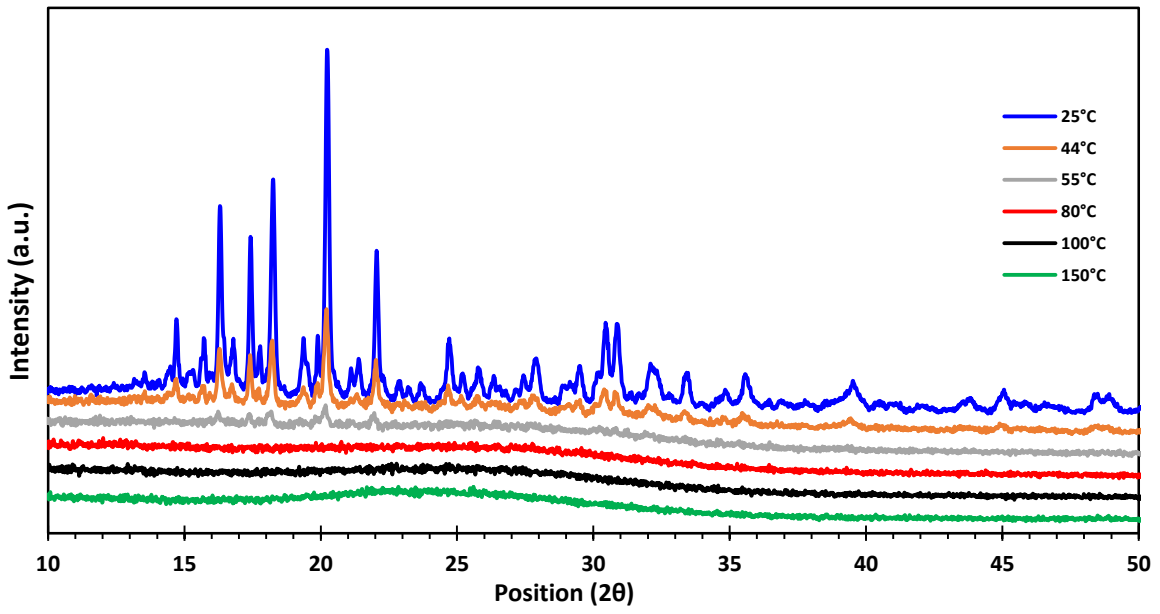

Figure 4. a) XRD patterns of HAP and its composites, b) Identification of $MgSO_4.6H_2O$ formation after 30h at ambient air exposition, c) In-situ XRD patterns of $MgSO_4.7H_2O$ during its dehydration from 25 to 150 °C.

In order to investigate the morphology and the salt deposition homogeneity, SEM analyses were performed. Based on **Figure 5** (**a and b**), different particle sizes with different morphologies have been observed for the both HAP composites. For more insight, the EDX mapping (**Figure 6**) have been performed in order to have an idea about the possible distribution of the salt on the HAP surface. As seen in **Figure 6**, the elements Mg and S were homogeneously distributed on the surface of the 5-$MgSO_4$/HAP. However, for the 20-$MgSO_4$/HAP sample (**Figure 7**), if the distribution of Mg and S elements on the surface was still homogenous on most of the HAP grains, some particles (highlighted by yellow dotted circles) presented a higher concentration of Mg and S, which relates to higher loading of $MgSO_4$ indicating the formation of salt aggregates on the surface of HAP. The presence of aggregates could potentially block the pore network, thus reducing the reaction surface between water vapor and salt.

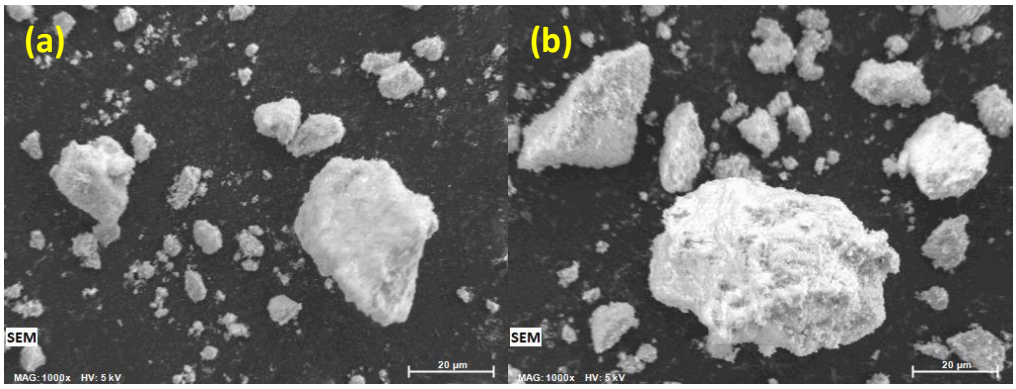

Figure 5. SEM images of a) 5-$MgSO_4$/HAP and b) 20-$MgSO_4$/HAP.

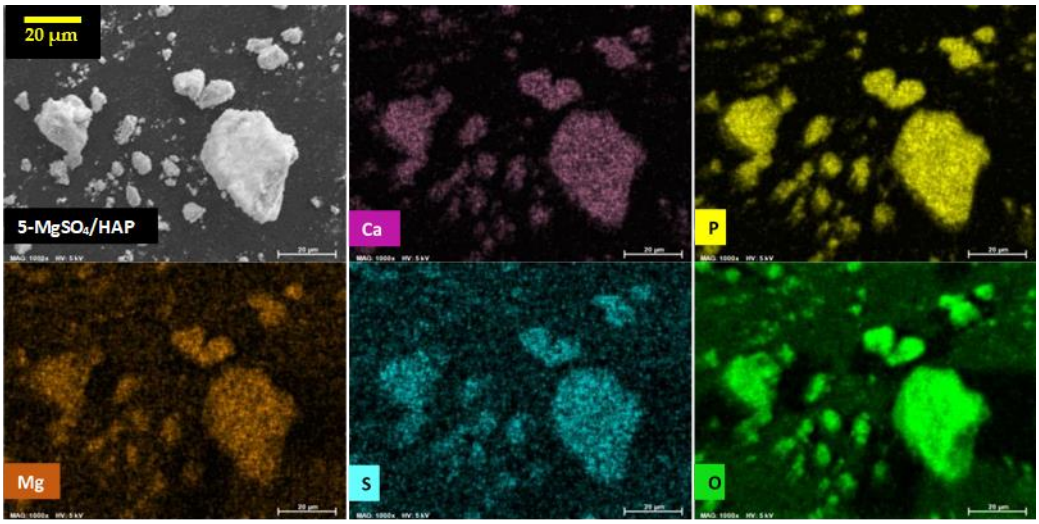

Figure 6. EDX mapping for 5-$MgSO_4$/HAP.

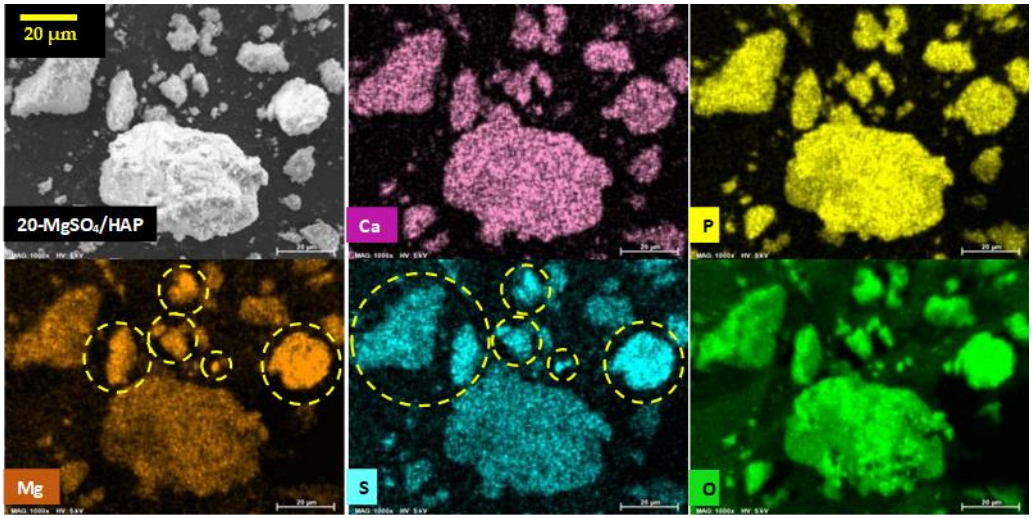

Figure 7. EDX mapping for 20-$MgSO_4$/HAP.

3.2. TG-DSC analysis for hydration behaviors

The hydration heat released and water sorption capacities of the HAP support and its composites were measured respectively by TG-DSC under controlled RH, regulated by a Wetsys apparatus. From the variation of the heat flow and the mass of the sample as a function of time, the heat released upon hydration (**Figure 8a**) and the water adsorption capacity (defined as "w_e" in Equation (1)) (**Figure 8b**) were deduced. The amount of heat produced and water uptake in both prepared composites increased as the salt concentration in the composites increased. This is probably due to the fact that,

the more salt was dispersed onto the porous structure, the more active sites were generated for the exothermic reaction between salt particles and water vapor. The hydration behavior of $MgSO_4$ was also experimented with the same temperature profile.

$$w_e = \frac{m_h - m_d}{m_d} \quad \textbf{(1)}$$

where w_e is the water adsorption capacity (g_{H2O}/g_{sample} or g/g in short), m_h (g) and m_d (g) correspond respectively to the final mass of the hydrated sample and the dehydrated sample. For $MgSO_4$, the water uptake is expressed as g_{H2O}/g of dehydrated salt and for the composite is expressed as g_{H2O}/g of dehydrated composite.

However, these values are lower than their respective calculated ones which are shown in **Table 2**. The calculated values are performed by simple addition of the contribution of the $MgSO_4$ salt and of the HAP support based on their respective content in the composites. This can be explained with the presence of the partially amorphous hydrated phases of $MgSO_4.yH_2O$ (absence of crystalline phase in the XRD patterns) [57,58]. The storage density of these partially hydrated are lower compared to the anhydrous $MgSO_4$, therefore the heat released of the composite is less significant. Moreover, the bare HAP presents a very low hydration heat that did not contribute greatly to the enhancement of heat storage density. Besides that, because of the pore blocking, there could be a certain amount of salt that cannot be reached by the water vapor (**Figure 8c**). Thus, the hydration energy released as well as the water uptake did not meet expectations. The performance of 20-$MgSO_4$/HAP was also compared with other sulfate-support composites previously reported in literatures. **Table 3** shows that the 20-$MgSO_4$/HAP has good energy storage density and has a potential to be a candidate for medium and low temperature applications.

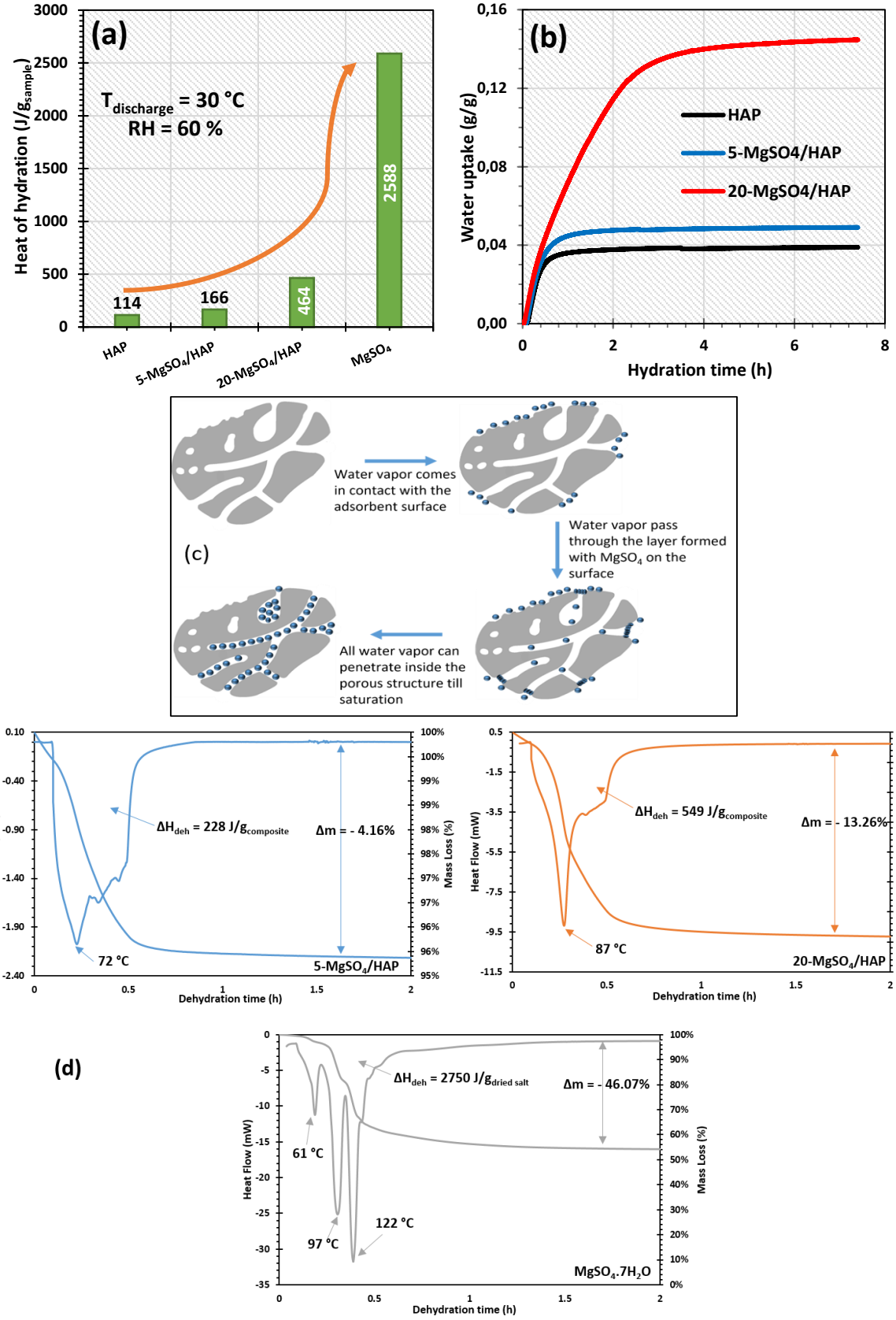

Figure 8. a) Hydration behavior of $MgSO_4$ and HAP composites at 30 °C and 60 %RH **b)** Water uptake curves of HAP support and composites ($T_{discharge}$ = 30 °C; RH = 60 %; 24 h of hydration c) Water adsorption mechanism on the storage material and d) Dehydration behaviour of $MgSO_4$ and HAP composites from 30 to 150 °C under dried air.

Figure 8d shows the dehydration behavior of $MgSO_4$ and HAP composites. The $MgSO_4.7H_2O$ decomposed at around 61 °C and produced an unstable phase that eventually decomposed to form $MgSO_4.H_2O$ with a mass loss of 46% and a dehydration enthalpy of 2.75 kJ/$g_{dried\ sallt}$. The difference in the behavior of the composites can be explained by the good dispersion of the salt into the HAP pore structure. The decrease in dehydration temperature can also be due to the change in their crystallinity after impregnation into the HAP support [59]. This result confirmed that the use of HAP can be beneficial for certain applications.

Table 2. Experimental results and calculated values of $MgSO_4$, HAP and its composites.

Sample	Heat released (J/g_{sample})	Heat released calculated (J/g_{sample})[b]	Water adsorption (g/g)	Water adsorption calculated (g/g)[b]
$MgSO_4$ [a]	2588	-	0.809	-
HAP	114	-	0.039	-
5-$MgSO_4$/HAP	166	216	0.049	0.071
20-$MgSO_4$/HAP	464	541	0.155	0.172

[a] Determined experimentally by TG-DSC/Wetsys.

[b] Calculated by addition of the heat contribution of $MgSO_4$ salt and HAP support in each sample.

Table 3. Performance comparison of 20-MgSO4/HAP and other sulfate-supported composites.

Material components	Operating conditions	Energy storage density (J/g)	Reference	Year
20-$MgSO_4$/HAP	**T_{hyd} = 30 °C; RH = 60 %**	**464**	**This paper**	
30-$MgSO_4$/Diatomite (D30)	T_{hyd} = 25 °C; RH = 80 %	460	[60]	2021
60-$MgSO_4$/Diatomite (D60)		773		
50-$MgSO_4$/Expanded graphite (EG50)	T_{hyd} = 25 °C; RH = 85 %	496.4	[61]	2021
$MgSO_4$/13x with %$MgSO_4$ up to 20%	T_{hyd} = 25 °C; RH = 60 %	510-575	[22]	2019
$MgSO_4$/zeolite (laboratory pilot)	T_{hyd} = 25 °C; RH = 85 %	401	[4]	2018
$MgSO_4$/zeolite Modernite	T_{hyd} = 22 °C; RH = 50 %	507	[62]	2013

3.3. Hydration kinetic modeling

Figure 9 shows the water uptake curves for the HAP support and two prepared composites. Similarly, they all display an initial short and fast water sorption rate during the first 30 minutes of hydration. However, after the initial fast adsorption, the kinetic curve of the 5-$MgSO_4$/HAP composite is similar to the curve of the support HAP which quickly reached the water sorption equilibrium only after 2 h of hydration. While for the 20-$MgSO_4$/HAP composite, after the initial fast adsorption, the kinetic curve slowed down significantly and then barely reached the equilibrium after over 7 h of hydration. This behavior is shown to be strongly impacted by the amount of salt deposited. When more salt was deposited, water vapor diffusion could become problematic as it takes more time for water vapor to reach entirely salt particles.

To investigate the kinetics of water uptake, several kinetic models were tested (**Table 4**). Among all of these kinetic equation models, six kinetic models showed a poor fiting based on on the correlation coefficient R^2: Elovich model (0.70-0.94), Vermeulen model (0.95-0.97) and Unipore model (0.17 -0.78). With the exception of the pseudo-first order (PFO) and pseudo-second order (PSO), which are two well-known kinetic models [63–65]. The fitting results are reported in **Figure 9** and the obtained kinetic parameters are listed in **Table 5.**

Table 4: Non-linear kinetic adsorption models.

Kinetic model	Equation	Description of parameters	Ref.
Pseudo First Order (PFO)	$w_t = w_e[1 - \exp(-K_1 t)]$	w_t is the water uptake at time t (g/g), w_e: the water uptake at equilibrium (g/g), t is the hydration time (h), K_1 and K_2 are respectively the rate constant of the PFO and PSO models (s^{-1}).	[63–65]
Pseudo Second Order (PSO)	$w_t = \frac{w_e^2 K_2 t}{1 + w_e K_2 t}$		
Elovich	$w_t = \frac{1}{\beta}\ln(\alpha\beta) + \frac{1}{\beta}\ln(t)$	α is the initial adsorption rate (mg/g min), and β is the extent of the surface coverage and activation energy of the process	[65,66]
Vermeulen	$w_t = w_e\sqrt{1 - \exp(-\frac{4\pi^2 D_v t}{d_p^2})}$ $K_v = \frac{4\pi^2 D_v}{d_p^2}$	Dv is the diffusion coefficient; dp is the particle radius	[67,68]
Unipore	$w_t = w_e \times 6\,(\frac{D_e \times t}{\pi})^{0.5}$	De is the the diffusion coefficient	[69]

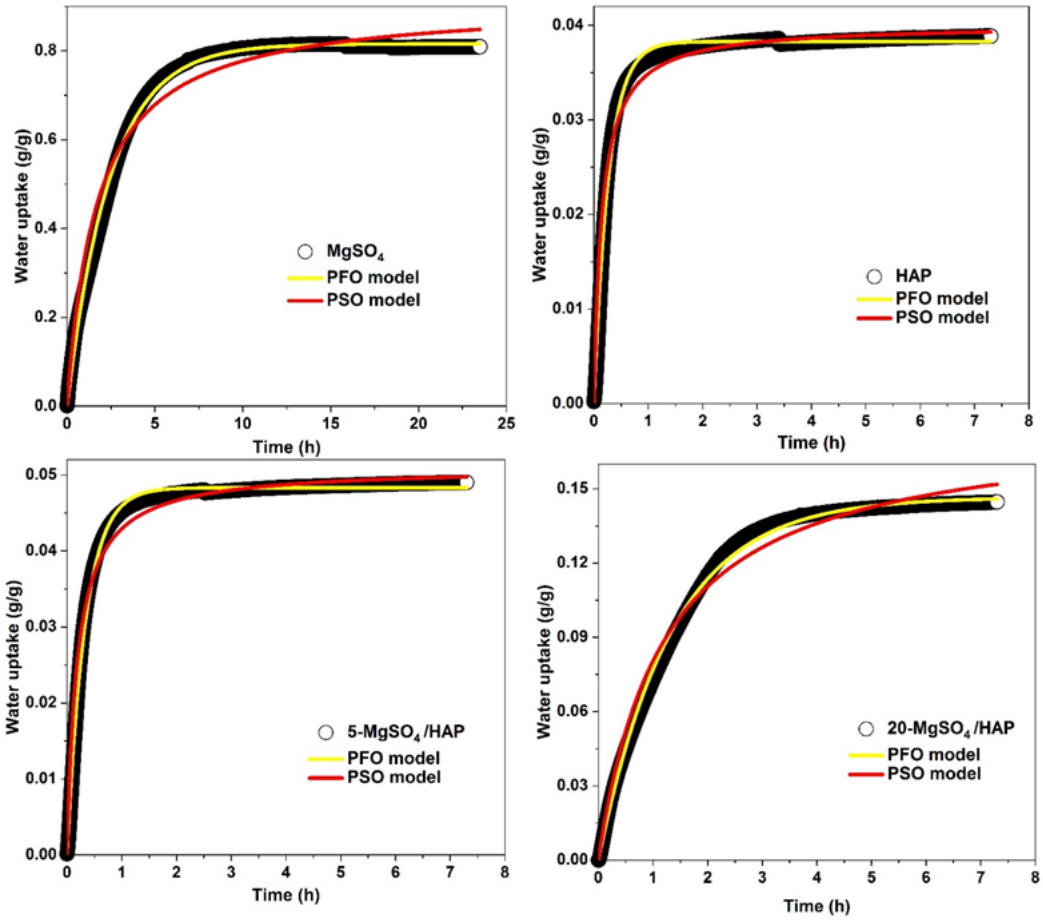

Figure 9. Adsorption kinetics fitting results of $MgSO_4$, HAP support and two composites with 5% and 20% salt content. (Hydration temperature: 30°C; RH: 60%; sample mass: ~10 mg; $MgSO_4$ denisty: 2.66 g/cm^3; HAP density: 3.16 g/cm^3; 20-$MgSO_4$/HAP density: 3.07 g/cm^3; 5-$MgSO_4$/HAP density: 3.14 g/cm^3).

Table 5. The kinetic parameters obtained by different adsorption kinetic models.

	$MgSO_4$	HAP	5-$MgSO_4$/HAP	20-$MgSO_4$/HAP
Pseudo-First-Order (PFO)				
We (g/g)	0.815	0.038	0.048	0.146
K_1 (10^{-4} s^{-1})	**1.133**	**10.24**	**8.347**	**2.069**
R^2	**0.996**	**0.988**	**0.993**	**0.997**
Pseudo-Second-Order (PSO)				
We (g/g)	0.909	0.040	0.051	0.176
K_2 (10^{-4} s^{-1})	1.794	462.5	288.1	13.16
R^2	0.957	0.953	0.962	0.977

It can be seen from **Figure 9** that the PFO model described better the adsorption processes of all samples than the PSO model (with R^2 coefficients of around 0.99). From the kinetic rate constant K_1 obtained from the PFO model, the hydration kinetics can be classified as following order (from fastest to slowest): HAP > 5-$MgSO_4$/HAP > 20-$MgSO_4$/HAP > $MgSO_4$. The $MgSO_4$ presents a slow kinetic compared to others materials (**Figure 9**). The salt required 15 hours to attain a stable hydration state, which is twice the rate of the 20-$MgSO_4$/HAP composite. This well-known slow hydration kinetic of the $MgSO_4$ was already investigated. According to Linnow et al. [15], when exposed to humid air, a thin layer of hydrated salt forms quickly on the support surface, restricting water vapor diffusion and thereby slowing the reaction rate. The HAP support presents a fastest kinetic which is probably due to the fast physical adsorption process during hydration. The impregnation of $MgSO_4$ has then a significant impact on this speed. In the case of the 5-$MgSO_4$/HAP composite, the kinetic was slightly impacted when the salt was integrated in the HAP porous structure. However, when the surface coverage of the salt was extended, as in the case of the 20-$MgSO_4$/HAP composite, the hydration kinetic significantly slows down (rate constant K_1 4 times lower) (**Figure 10**). As aforementioned, these behaviors are related to the difficulty of water vapor to diffuse inside the material pore network, in particular composites with higher salt content. Another result is that the slow kinetic of $MgSO_4$ was greatly improved as it was dispersed in the porous matrix HAP (the kinetic rate constant of the composites are higher than $MgSO_4$). This latter could have a remarkable value in residential applications, because it will reduce considerably the hydration time and thus improve the operating flexibility of the overall storage system.

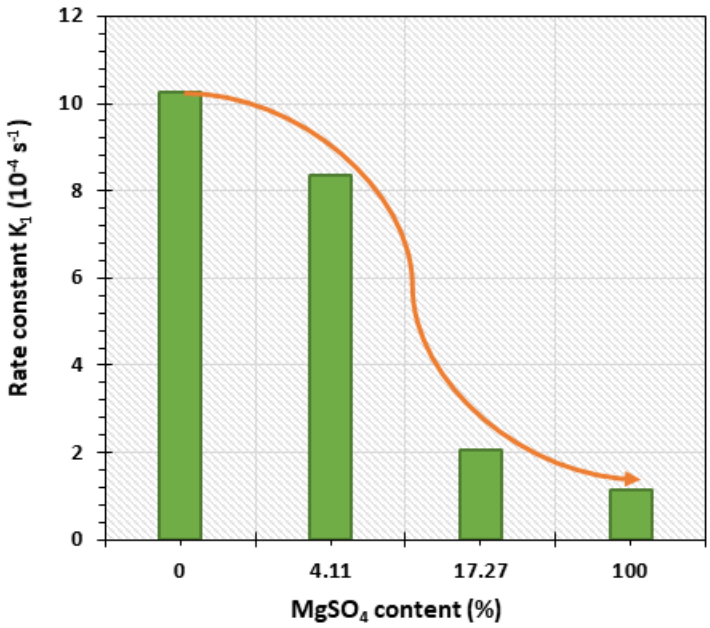

476

477 **Figure 10.** Influence of the salt content on the kinetic rate constants.

478

479 **3.3. Cyclability and stability**

480 To evaluate the cyclability and stability of the 20-$MgSO_4$/HAP composite, the sample
481 has been exposed to a short-cycle hydration/dehydration treatment consisting of 20
482 cycles between temperatures of 150 °C (Dehydration) and 30 °C (Hydration, at a
483 relative humidity of 60%). In the following step, the heat released for each cycle has
484 been determined as a first benchmark. As it can be seen in **Figure 11**, there is only a
485 small fluctuations of heat released between each cycle, which confirms the good
486 stability with an average ESD of 472 J/g.

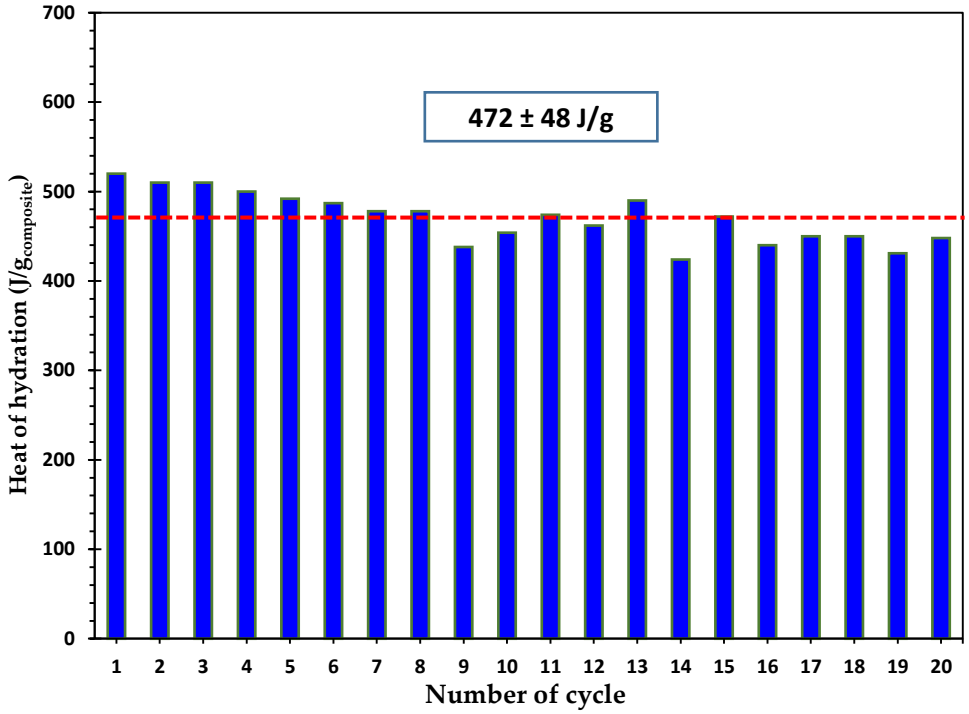

Figure 11. Evaluation of 20-$MgSO_4$/HAP composite stability for 20 cycles of hydration/dehydration.

Figure 12 shows the TGA signals during hydration and dehydration of 5 different cycles in the cyclability test (1^{st}, 5^{th}, 10^{th}, 17^{th}, 20^{th}). During the hydration reactions, a degradation in water uptake during the first 10 cycles is noted, from 0.188 g/g in the first hydration but down to 0.157 g/g after the 10^{th} hydration. From this point onwards, the water adsorption capacity is stabilized at 0.157 g/g (83.5% compared to 0.188 g/g) until the 20^{th} hydration. The hydration kinetic rate is also reported to be stable at around $1.2.10^{-4}$ s^{-1} during the cycling experiment.

In terms of dehydration reactions, a loss of 13.26% in mass is recorded in the first dehydration. Over cycling, the dehydration becomes less and less effective, but not significantly since during the last dehydration, a loss of 11.55% (about 87.1% compared to 13.26%) in mass is reported.

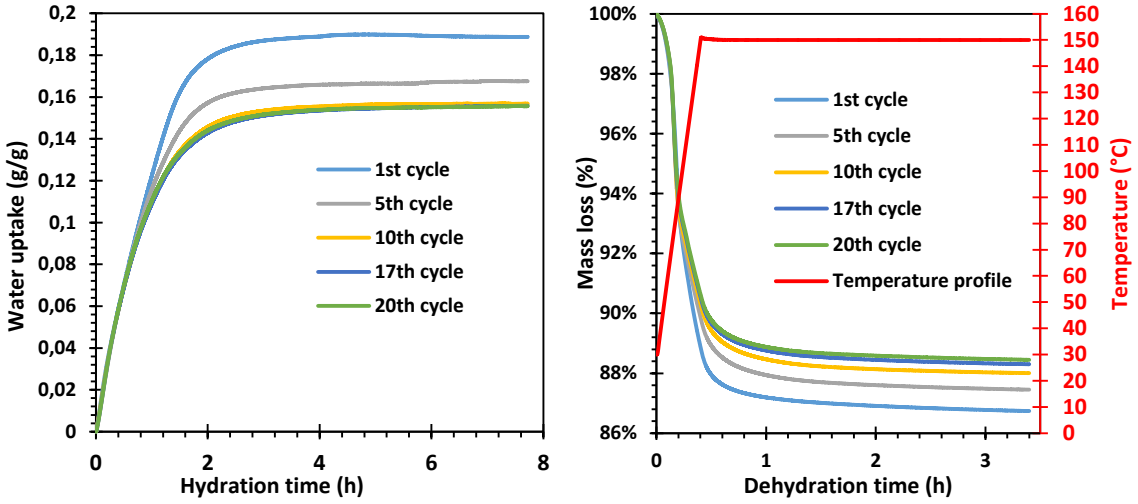

Figure 12. TGA curves of 5 different cycles during the cyclability experiment (1st, 5th, 10th, 17th, 20th).

The SEM and EDX mapping (**Figure 13**) of sample after 20 cycles have been done to verify if there are any changes in term of salts distribution, agglomeration and so on. The results showed that there is no significance difference before and after cycling experiment, which confirm also the morphological stability of the composites. Consequently, these composites can be a base for the development of potential material for TCHS application based on HAP. A research regarding the development of new composites on other HAP types with the objective to enhance the water uptake and increase the amount of deposited salt in order to improve the thermal storage capacity is ongoing.

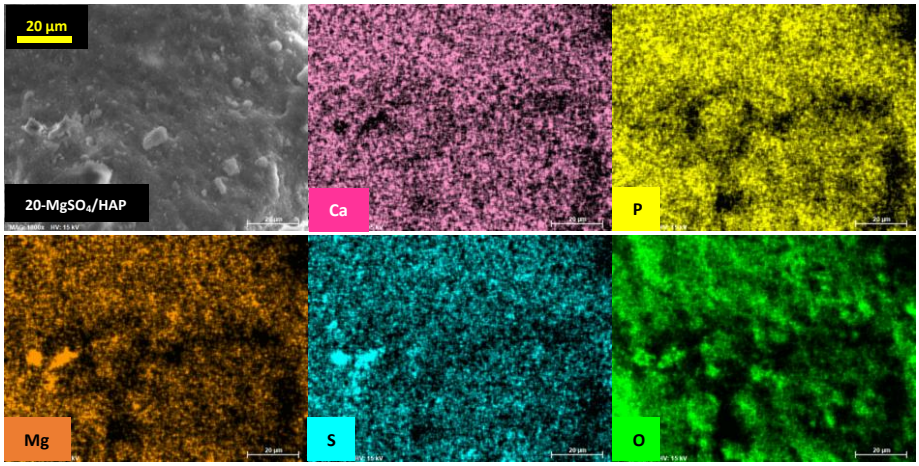

Figure 13. EDX mapping for 20-$MgSO_4$/HAP after 20 cycles.

4. Conclusions

Wide pore hydroxyapatite composite materials impregnated with different amounts of $MgSO_4$, as prospective thermochemical seasonal heat storage materials, have been studied using the TG-DSC apparatus. Despite the fact that magnesium sulfate was unable to fully exploit its sorption capacities, a composite containing 20% $MgSO_4$ produced the maximum heat (464 J/g) as compared to HAP impregnated with 5% $MgSO_4$ (166 J/g). The excellent dispersion of $MgSO_4$ increases the storing capability of composite materials. High heat and water storage capabilities are not the only factors to consider when selecting a storage material in thermochemical heat storage systems. A rapid water sorption kinetics is also necessary for the system's usability. Good fitting of the kinetic experimental data with the model equation has been successfully performed, allowing us to determine the rate controlling adsorption mechanism, which is an important factor in thermochemical heat storage system design. The repeated stability of $MgSO_4$-HAP is evaluated, revealing that this two-component sorbent is relatively well constant after 20 dehydration/hydration cycles. In perspective, these promising results open the way to the optimization of a new thermochemical heat storage composite materials' family based on HAP. New HAP compositions and morphology can be then studied in order to improve the salt dispersion and the water mass transfer.

Author Contributions: Conceptualization and Writing—Original Draft Preparation M. H. N, S.B.; Methodology and Writing—Original Draft Preparation M.Z; Review & Editing-Supervision, S. B., P. D; Preparation of hydroxyapatite material, A. G; Nitrogen physisorption analyses, M.H.N, C. V; Writing—Review & Editing, Supervision, and Project Administration S. B. All authors have read and agreed to the published version of the manuscript.

Funding: - Region Grand Est for providing funding for the acquisition of the TG-DSC equipment within the "STOCKFATAL" project and for the contribution to Mr. Minh Hoang Nguyen's thesis grant.

- Carnot MICA for funding part of this study in the frame of the STOCKENER project.

- IS2M for the postdoctoral grant of M. Zbair in the frame of the "Projets Structurants" call.

Institutional Review Board Statement: Not applicable.

Informed Consent Statement: Not applicable.

Data Availability Statement: Not applicable.

Acknowledgments: The authors would like to thank the Carnot Institutes MICA(France) for supporting a part of this study within the STOCKENER; Region Grand Est (France) for providing funding for the acquisition of the TG-DSC equipment, in the frame of STOCKFATAL project, and financing a part of the PhD-grant of Mr. Minh Hoang Nguyen.

All physicochemical characterizations were performed on the IS2M technical platforms. The authors are very grateful to L. Michelin (XRF) and L. Josien (SEM+EDX) for their contribution.

Conflicts of Interest: The authors declare no conflict of interest.

Nomenclature

TES, thermal energy system;

TCHS, thermochemical heat storage;

HAP, hydroxyapatite;

IWI, Incipient Wetness Impregnation;

XRD, X-ray Diffraction;

WDXRF, wavelength-dispersive X-Ray Fluorescence;

SEM, Scanning Electron Microscope;

EDX, Energy Dispersive X-ray;

BET, Brunauer, Emmett and Teller;

570 PSD, pore size distribution;

571 BJH, Barrett, Joyner and Halenda;

572 TG, thermogravimetry;

573 DSC, Differential Scanning Calorimetry;

574 RH, relative humidity;

575 PFO, pseudo-first order;

576 PSO, pseudo-second order.

577 ## References

578 [1] F.J. Barba, M. Gavahian, I. Es, Z. Zhu, F. Chemat, J.M. Lorenzo, A. Mousavi Khaneghah, Solar radiation as a
579 prospective energy source for green and economic processes in the food industry: From waste biomass valorization to
580 dehydration, cooking, and baking, J. Clean. Prod. 220 (2019) 1121–1130. https://doi.org/10.1016/j.jclepro.2019.02.175.

581 [2] A.V. da Rosa, J.C. Ordóñez, Storage of Energy, in: Fundam. Renew. Energy Process., Elsevier, 2022: pp. 855–896.
582 https://doi.org/10.1016/B978-0-12-816036-7.00031-2.

583 [3] G. Airò Farulla, M. Cellura, F. Guarino, M. Ferraro, A Review of Thermochemical Energy Storage Systems for Power
584 Grid Support, Appl. Sci. 10 (2020) 3142. https://doi.org/10.3390/app10093142.

585 [4] C. Xu, Z. Yu, Y. Xie, Y. Ren, F. Ye, X. Ju, Study of the hydration behavior of zeolite-MgSO4 composites for long-term
586 heat storage, Appl. Therm. Eng. 129 (2018) 250–259. https://doi.org/10.1016/j.applthermaleng.2017.10.031.

587 [5] A Comprehensive Review of Thermal Energy Storage, Sustainability. 10 (2018) 191. https://doi.org/10.3390/su10010191.

588 [6] W. Li, M. Zeng, Q. Wang, Development and performance investigation of MgSO4/SrCl2 composite salt hydrate for
589 mid-low temperature thermochemical heat storage, Sol. Energy Mater. Sol. Cells. 210 (2020) 110509.
590 https://doi.org/10.1016/j.solmat.2020.110509.

591 [7] G.T. Whiting, D. Grondin, D. Stosic, S. Bennici, A. Auroux, Zeolite–MgCl2 composites as potential long-term heat
592 storage materials: Influence of zeolite properties on heats of water sorption, Sol. Energy Mater. Sol. Cells. 128 (2014)
593 289–295. https://doi.org/10.1016/j.solmat.2014.05.016.

594 [8] H. Wu, F. Salles, J. Zajac, A Critical Review of Solid Materials for Low-Temperature Thermochemical Storage of Solar
595 Energy Based on Solid-Vapour Adsorption in View of Space Heating Uses, Molecules. 24 (2019) 945.
596 https://doi.org/10.3390/molecules24050945.

597 [9] P. Tatsidjodoung, N. Le Pierrès, L. Luo, A review of potential materials for thermal energy storage in building
598 applications, Renew. Sustain. Energy Rev. 18 (2013) 327–349. https://doi.org/10.1016/j.rser.2012.10.025.

599 [10] L.G. Gordeeva, Y.D. Tu, Q. Pan, M.L. Palash, B.B. Saha, Y.I. Aristov, R.Z. Wang, Metal-organic frameworks for energy
600 conversion and water harvesting: A bridge between thermal engineering and material science, Nano Energy. 84 (2021)
601 105946. https://doi.org/10.1016/j.nanoen.2021.105946.

[11] M. Zbair, S. Bennici, Survey Summary on Salts Hydrates and Composites Used in Thermochemical Sorption Heat Storage: A Review, Energies. 14 (2021) 3105. https://doi.org/10.3390/en14113105.

[12] S.Z. Xu, Lemington, R.Z. Wang, L.W. Wang, J. Zhu, A zeolite 13X/magnesium sulfate–water sorption thermal energy storage device for domestic heating, Energy Convers. Manag. 171 (2018) 98–109. https://doi.org/10.1016/j.enconman.2018.05.077.

[13] K.E. N'Tsoukpoe, T. Schmidt, H.U. Rammelberg, B.A. Watts, W.K.L. Ruck, A systematic multi-step screening of numerous salt hydrates for low temperature thermochemical energy storage, Appl. Energy. 124 (2014) 1–16. https://doi.org/10.1016/j.apenergy.2014.02.053.

[14] H. Ait Ousaleh, S. Sair, S. Mansouri, Y. Abboud, A. Faik, A. El Bouari, New hybrid graphene/inorganic salt composites for thermochemical energy storage: Synthesis, cyclability investigation and heat exchanger metal corrosion protection performance, Sol. Energy Mater. Sol. Cells. 215 (2020) 110601. https://doi.org/10.1016/j.solmat.2020.110601.

[15] K. Linnow, M. Niermann, D. Bonatz, K. Posern, M. Steiger, Experimental Studies of the Mechanism and Kinetics of Hydration Reactions, Energy Procedia. 48 (2014) 394–404. https://doi.org/10.1016/j.egypro.2014.02.046.

[16] K.-D. Grevel, J. Majzlan, A. Benisek, E. Dachs, M. Steiger, A.D. Fortes, B. Marler, Experimentally Determined Standard Thermodynamic Properties of Synthetic MgSO 4 ·4H 2 O (Starkeyite) and MgSO 4 ·3H 2 O: A Revised Internally Consistent Thermodynamic Data Set for Magnesium Sulfate Hydrates, Astrobiology. 12 (2012) 1042–1054. https://doi.org/10.1089/ast.2012.0823.

[17] T. Yan, T. Li, J. Xu, J. Chao, R. Wang, Y.I. Aristov, L.G. Gordeeva, P. Dutta, S.S. Murthy, Ultrahigh-Energy-Density Sorption Thermal Battery Enabled by Graphene Aerogel-Based Composite Sorbents for Thermal Energy Harvesting from Air, ACS Energy Lett. 6 (2021) 1795–1802. https://doi.org/10.1021/acsenergylett.1c00284.

[18] Y.. Aristov, G. Restuccia, G. Cacciola, V.. Parmon, A family of new working materials for solid sorption air conditioning systems, Appl. Therm. Eng. 22 (2002) 191–204. https://doi.org/10.1016/S1359-4311(01)00072-2.

[19] L. Silvester, Q. Touloumet, A. Kamaruddin, F. Chassagneux, G. Postole, A. Auroux, L. Bois, Influence of Silica Functionalization on Water Sorption and Thermochemical Heat Storage of Mesoporous SBA-15/CaCl 2 Composites, ACS Appl. Energy Mater. 4 (2021) 5944–5956. https://doi.org/10.1021/acsaem.1c00786.

[20] E. Courbon, P. D'Ans, A. Permyakova, O. Skrylnyk, N. Steunou, M. Degrez, M. Frère, A new composite sorbent based on SrBr2 and silica gel for solar energy storage application with high energy storage density and stability, Appl. Energy. 190 (2017) 1184–1194. https://doi.org/10.1016/j.apenergy.2017.01.041.

[21] B. Ding, C. Xu, Z. Liao, F. Ye, Study on long-term thermochemical thermal storage performance based on SrBr2-expanded vermiculite composite materials, J. Energy Storage. 42 (2021) 103081. https://doi.org/10.1016/j.est.2021.103081.

[22] Q. Wang, Y. Xie, B. Ding, G. Yu, F. Ye, C. Xu, Structure and hydration state characterizations of MgSO4-zeolite 13x composite materials for long-term thermochemical heat storage, Sol. Energy Mater. Sol. Cells. 200 (2019) 110047. https://doi.org/10.1016/j.solmat.2019.110047.

[23] J.X. Xu, T.X. Li, J.W. Chao, T.S. Yan, R.Z. Wang, High energy-density multi-form thermochemical energy storage based on multi-step sorption processes, Energy. 185 (2019) 1131–1142. https://doi.org/https://doi.org/10.1016/j.energy.2019.07.076.

[24] W. Shi, Y. Zhu, C. Shen, J. Shi, G. Xu, X. Xiao, R. Cao, Water sorption properties of functionalized MIL-101(Cr)-X (X=-NH2, –SO3H, H, –CH3, –F) based composites as thermochemical heat storage materials, Microporous Mesoporous Mater. 285 (2019) 129–136. https://doi.org/10.1016/j.micromeso.2019.05.003.

[25] A.I. Shkatulov, J. Houben, H. Fischer, H.P. Huinink, Stabilization of K2CO3 in vermiculite for thermochemical energy storage, Renew. Energy. 150 (2020) 990–1000. https://doi.org/10.1016/j.renene.2019.11.119.

[26] H. Ait Ousaleh, S. Sair, A. Zaki, A. Younes, A. Faik, A. El Bouari, Advanced experimental investigation of double hydrated salts and their composite for improved cycling stability and metal compatibility for long-term heat storage technologies, Renew. Energy. 162 (2020) 447–457. https://doi.org/10.1016/j.renene.2020.08.085.

[27] W. Li, J.J. Klemeš, Q. Wang, M. Zeng, Development and characteristics analysis of salt-hydrate based composite sorbent for low-grade thermochemical energy storage, Renew. Energy. 157 (2020) 920–940. https://doi.org/10.1016/j.renene.2020.05.062.

[28] T.S. Yan, T.X. Li, J.X. Xu, R.Z. Wang, Water sorption properties, diffusion and kinetics of zeolite NaX modified by ion-exchange and salt impregnation, Int. J. Heat Mass Transf. 139 (2019) 990–999. https://doi.org/10.1016/j.ijheatmasstransfer.2019.05.080.

[29] P. D'Ans, E. Courbon, A. Permyakova, F. Nouar, C. Simonnet-Jégat, F. Bourdreux, L. Malet, C. Serre, M. Frère, N. Steunou, A new strontium bromide MOF composite with improved performance for solar energy storage application, J. Energy Storage. 25 (2019) 100881. https://doi.org/10.1016/j.est.2019.100881.

[30] D. Mahon, P. Henshall, G. Claudio, P.C. Eames, Feasibility study of MgSO4 + zeolite based composite thermochemical energy stores charged by vacuum flat plate solar thermal collectors for seasonal thermal energy storage, Renew. Energy. 145 (2020) 1799–1807. https://doi.org/10.1016/j.renene.2019.05.135.

[31] W. Li, J.J. Klemeš, Q. Wang, M. Zeng, Salt hydrate–based gas-solid thermochemical energy storage: Current progress, challenges, and perspectives, Renew. Sustain. Energy Rev. 154 (2022) 111846. https://doi.org/10.1016/j.rser.2021.111846.

[32] J. Lin, Q. Zhao, H. Huang, H. Mao, Y. Liu, Y. Xiao, Applications of low-temperature thermochemical energy storage systems for salt hydrates based on material classification: A review, Sol. Energy. 214 (2021) 149–178. https://doi.org/10.1016/j.solener.2020.11.055.

[33] Z. Xueling, W. Feifei, Z. Qi, L. Xudong, W. Yanling, Z. Yeqiang, C. Chuanxiao, J. Tingxiang, Heat storage performance analysis of ZMS-Porous media/CaCl2/MgSO4 composite thermochemical heat storage materials, Sol. Energy Mater. Sol. Cells. 230 (2021) 111246. https://doi.org/10.1016/j.solmat.2021.111246.

[34] J. Jänchen, H. Stach, Adsorption properties of porous materials for solar thermal energy storage and heat pump applications, Energy Procedia. 30 (2012) 289–293. https://doi.org/10.1016/j.egypro.2012.11.034.

[35] I.V. Ponomarenko, I.S. Glaznev, A.V. Gubar, Y.I. Aristov, S.D. Kirik, Synthesis and water sorption properties of a new composite "CaCl2 confined into SBA-15 pores," Microporous Mesoporous Mater. 129 (2010) 243–250. https://doi.org/10.1016/j.micromeso.2009.09.023.

[36] E. Courbon, P. D'Ans, A. Permyakova, O. Skrylnyk, N. Steunou, M. Degrez, M. Frère, Further improvement of the synthesis of silica gel and CaCl2 composites: Enhancement of energy storage density and stability over cycles for solar heat storage coupled with space heating applications, Sol. Energy. 157 (2017) 532–541. https://doi.org/10.1016/j.solener.2017.08.034.

[37] G. Whiting, D. Grondin, S. Bennici, A. Auroux, Heats of water sorption studies on zeolite–MgSO4 composites as potential thermochemical heat storage materials, Sol. Energy Mater. Sol. Cells. 112 (2013) 112–119. https://doi.org/10.1016/j.solmat.2013.01.020.

[38] L.G. Gordeeva, Y.I. Aristov, Composites 'salt inside porous matrix' for adsorption heat transformation: a current state-of-the-art and new trends, Int. J. Low-Carbon Technol. 7 (2012) 288–302. https://doi.org/10.1093/ijlct/cts050.

[39] V. Palomba, A. Sapienza, Y. Aristov, Dynamics and useful heat of the discharge stage of adsorptive cycles for long term thermal storage, Appl. Energy. 248 (2019) 299–309. https://doi.org/10.1016/j.apenergy.2019.04.134.

[40] L. Calabrese, V. Brancato, V. Palomba, A. Frazzica, L.F. Cabeza, Magnesium sulphate-silicone foam composites for thermochemical energy storage: Assessment of dehydration behaviour and mechanical stability, Sol. Energy Mater. Sol. Cells. 200 (2019) 109992. https://doi.org/10.1016/j.solmat.2019.109992.

[41] A. Jabbari-Hichri, S. Bennici, A. Auroux, CaCl2-containing composites as thermochemical heat storage materials, Sol. Energy Mater. Sol. Cells. 172 (2017) 177–185. https://doi.org/10.1016/j.solmat.2017.07.037.

[42] L.G. Gordeeva, Y.I. Aristov, Composites 'salt inside porous matrix' for adsorption heat transformation: a current state-of-the-art and new trends, Int. J. Low-Carbon Technol. 7 (2012) 288–302. https://doi.org/10.1093/ijlct/cts050.

[43] J.A. Lett, M. Sundareswari, K. Ravichandran, M.B. Latha, S. Sagadevan, M.R. Bin Johan, Tailoring the morphological features of sol–gel synthesized mesoporous hydroxyapatite using fatty acids as an organic modifier, RSC Adv. 9 (2019) 6228–6240. https://doi.org/10.1039/C9RA00051H.

[44] H. Li, D. Wu, J. Wu, L.-Y. Dong, Y.-J. Zhu, X. Hu, Flexible, High-Wettability and Fire-Resistant Separators Based on Hydroxyapatite Nanowires for Advanced Lithium-Ion Batteries, Adv. Mater. 29 (2017) 1703548. https://doi.org/10.1002/adma.201703548.

[45] N.A. Medellin-Castillo, R. Leyva-Ramos, E. Padilla-Ortega, R.O. Perez, J.V. Flores-Cano, M.S. Berber-Mendoza, Adsorption capacity of bone char for removing fluoride from water solution. Role of hydroxyapatite content, adsorption mechanism and competing anions, J. Ind. Eng. Chem. 20 (2014) 4014–4021. https://doi.org/10.1016/j.jiec.2013.12.105.

[46] M. Ibrahim, M. Labaki, J.-M. Giraudon, J.-F. Lamonier, Hydroxyapatite, a multifunctional material for air, water and soil pollution control: A review, J. Hazard. Mater. 383 (2020) 121139. https://doi.org/10.1016/j.jhazmat.2019.121139.

[47] A. Amedlous, O. Amadine, Y. Essamlali, H. Maati, N. Semlal, M. Zahouily, Copper Loaded Hydroxyapatite Nanoparticles as eco-friendly Fenton-like catalyst to Effectively Remove Organic Dyes, J. Environ. Chem. Eng. 9 (2021) 105501. https://doi.org/10.1016/j.jece.2021.105501.

[48] Y. Wang, D. Liang, F. Liu, W. Zhang, X. Di, C. Wang, A polyethylene glycol/hydroxyapatite composite phase change material for thermal energy storage, Appl. Therm. Eng. 113 (2017) 1475–1482. https://doi.org/10.1016/j.applthermaleng.2016.11.159.

[49] Y. Wu, C. Wang, J. Li, Y. Li, Porous Hydroxyapatite Foams: Excellent Carrier of Hydrated Salt with Adjustable Pores for Thermal Energy Storage, Ind. Eng. Chem. Res. 60 (2021) 1259–1265. https://doi.org/10.1021/acs.iecr.0c05480.

[50] S. Campisi, C. Castellano, A. Gervasini, Tailoring the structural and morphological properties of hydroxyapatite materials to enhance the capture efficiency towards copper(<scp>ii</scp>) and lead(<scp>ii</scp>) ions, New J. Chem. 42 (2018) 4520–4530. https://doi.org/10.1039/C8NJ00468D.

[51] P. Munnik, P.E. de Jongh, K.P. de Jong, Recent Developments in the Synthesis of Supported Catalysts, Chem. Rev. 115 (2015) 6687–6718. https://doi.org/10.1021/cr500486u.

[52] P.A.J. Donkers, L.C. Sögütoglu, H.P. Huinink, H.R. Fischer, O.C.G. Adan, A review of salt hydrates for seasonal heat storage in domestic applications, Appl. Energy. 199 (2017) 45–68. https://doi.org/10.1016/j.apenergy.2017.04.080.

[53] S. Bennici, T. Polimann, M. Ondarts, E. Gonze, C. Vaulot, N. Le Pierrès, Long-term impact of air pollutants on thermochemical heat storage materials, Renew. Sustain. Energy Rev. 117 (2020) 109473. https://doi.org/10.1016/j.rser.2019.109473.

[54] F. Rouquerol, J. Rouquerol, K. Sing, Assessment of Mesoporosity, in: Adsorpt. by Powders Porous Solids, Elsevier, 1999: pp. 191–217. https://doi.org/10.1016/B978-012598920-6/50008-7.

[55] M. Thommes, K. Kaneko, A. V. Neimark, J.P. Olivier, F. Rodriguez-Reinoso, J. Rouquerol, K.S.W. Sing, Physisorption of gases, with special reference to the evaluation of surface area and pore size distribution (IUPAC Technical Report), Pure Appl. Chem. 87 (2015) 1051–1069. https://doi.org/10.1515/pac-2014-1117.

[56] I.C. Medeiros-Costa, C. Laroche, J. Pérez-Pellitero, B. Coasne, Characterization of hierarchical zeolites: Combining adsorption/intrusion, electron microscopy, diffraction and spectroscopic techniques, Microporous Mesoporous Mater. 287 (2019) 167–176. https://doi.org/10.1016/j.micromeso.2019.05.057.

[57] V.M. van Essen, H.A. Zondag, J.C. Gores, L.P.J. Bleijendaal, M. Bakker, R. Schuitema, W.G.J. van Helden, Z. He, C.C.M. Rindt, Characterization of MgSO4 Hydrate for Thermochemical Seasonal Heat Storage, J. Sol. Energy Eng. 131 (2009). https://doi.org/10.1115/1.4000275.

[58] D.T. Vaniman, D.L. Bish, S.J. Chipera, C.I. Fialips, J. William Carey, W.C. Feldman, Magnesium sulphate salts and the history of water on Mars, Nature. 431 (2004) 663–665. https://doi.org/10.1038/nature02973.

[59] H. Zhou, D. Zhang, Effect of graphene oxide aerogel on dehydration temperature of graphene oxide aerogel stabilized MgCl2·6H2O composites, Sol. Energy. 184 (2019) 202–208. https://doi.org/10.1016/j.solener.2019.03.076.

[60] Y. Zhang, Q. Miao, X. Jia, Y. Jin, Z. Li, L. Tan, Y. Ding, Diatomite-based magnesium sulfate composites for thermochemical energy storage: Preparation and performance investigation, Sol. ENERGY. 224 (2021) 907–915. https://doi.org/10.1016/j.solener.2021.05.054.

[61] Q. Miao, Y. Zhang, X. Jia, L. Tan, Y. Ding, MgSO4-expanded graphite composites for mass and heat transfer enhancement of thermochemical energy storage, Sol. Energy. 220 (2021) 432–439. https://doi.org/10.1016/j.solener.2021.03.008.

[62] G. Whiting, D. Grondin, S. Bennici, A. Auroux, Heats of water sorption studies on zeolite-MgSO4 composites as potential thermochemical heat storage materials, Sol. Energy Mater. Sol. Cells. (2013). https://doi.org/10.1016/j.solmat.2013.01.020.

[63] S. Langergen, B.K. Svenska, Zur theorie der sogenannten adsoption geloester stoffe, Vetensk. Handl. 24 (1898) 1–39.

[64] G. McKay, Pseudo-second order model for sorption processes, Proc Biochem. 34 (1999) 451.

[65] H.N. Tran, S.J. You, A. Hosseini-Bandegharaei, H.P. Chao, Mistakes and inconsistencies regarding adsorption of contaminants from aqueous solutions: A critical review, Water Res. 120 (2017) 88–116. https://doi.org/10.1016/j.watres.2017.04.014.

[66] I.S. MCLINTOCK, The Elovich Equation in Chemisorption Kinetics, Nature. 216 (1967) 1204–1205. https://doi.org/10.1038/2161204a0.

[67] M. Balsamo, F. Montagnaro, Fractal-like Vermeulen Kinetic Equation for the Description of Diffusion-Controlled Adsorption Dynamics, J. Phys. Chem. C. 119 (2015) 8781–8785. https://doi.org/10.1021/acs.jpcc.5b01783.

[68] T. Vermeulen, Theory for Irreversible and Constant-Pattern Solid Diffusion, Ind. Eng. Chem. 45 (1953) 1664–1670. https://doi.org/10.1021/ie50524a025.

[69] A. Davarpanah, B. Mirshekari, Experimental Investigation and Mathematical Modeling of Gas Diffusivity by Carbon Dioxide and Methane Kinetic Adsorption, Ind. Eng. Chem. Res. 58 (2019) 12392–12400. https://doi.org/10.1021/acs.iecr.9b01920.